systematic uncertainties. There is good agreement between the two data points for K_3C_{60} (19 K and 14.24 Å) and Rb_3C_{60} (29.6 K and 14.42 Å) at 1 bar. The absolute uncertainties (±0.5 K %) are smaller than the plot symbols.

The solid curve in Fig. 2 indicates that all three data sets are represented reasonably well by a single quadratic function. We conclude that the proposed universal correlation between T_c and a is correct to first order. The positive sign of the quadratic term may serve as a detailed test of competing models, for example, from the dependence on a of the parameters in the MacMillan formula.

Our data also reveal a small second-order intercalate-specific contribution to $T_c(a)$. From Fig. 1, the compressibilities of K_3C_{60} and Rb_3C_{60} are not identical, as would be required by a strictly universal correlation. The three data sets in Fig. 2 can also be reasonably well described by individual linear segments. The "universal" slope of Fleming's directly measured values is 50 K $Å^{-1}$, which is quite close to our value of 45 ± 1 K $Å^{-1}$ for Rb_3C_{60} but significantly larger than our value of 33 ± 2 K $Å^{-1}$ for K_3C_{60}. The intercalate-specific effect is only significant at small a, that is, at large intermolecular overlap.

The sense of this effect is inconsistent with a proposal that metal-C_{60} optic modes are responsible for the pairing interaction (*13*). In this hypothesis, superconductivity arises from strong coupling to relatively low-frequency modes rather than from weak coupling to the intramolecular vibrations, which lie at higher frequencies (*14, 15*). If we assume a linear contribution to $T_c(a)$ from the $e^{1/VN(E_F)}$ factor independent of chemical composition, and that the important coupling phonons are zone-boundary optic modes involving planes of M_3 and of C_{60} (*13*), there would be an additional scaling of T_c as $\sqrt{(1/m)}$, where m is the reduced mass. This scaling would be in the ratio 14:10 for K_3C_{60} and Rb_3C_{60}, the inverse of the observed 33:45 ratio of slopes.

There are several possible origins for the small intercalate-specific contribution. The first is suggested by the complex Fermi surface of K_3C_{60} (*16*). In addition to bandwidth variations, which depend directly on the lattice parameter, the volume of the Fermi surface may be subtly different for different intercalates, or may vary with lattice parameter or pressure, or both effects could occur. Another possibility is a pressure-induced phase transition involving molecular orientations. In pure C_{60}, free molecular rotations freeze out at T_{mo} = 249 K at 1 bar, locking into specific orientations with respect to the crystal axes (*17*), and T_{mo} decreases rapidly with increasing P (*18, 19*). An x-ray study of K_3C_{60} indicates two equally populated molecular orientations at 300 K and 1 bar (*20*), and a nuclear magnetic resonance study of Rb_3C_{60} gives evidence for a transition near 300 K (*21*). It is therefore likely that M_3C_{60} transforms to an orientationally ordered phase at 300 K within the P range of the present data, which could affect our analysis by introducing discontinuities in $a(P)$ or by slightly modifying the Fermi surface. The diffraction signature of this transition is quite subtle in C_{60} (*17*) and would have been undetectable in the present experiments. More data at the extremes of a would help clarify the situation, for example dT_c/dP and compressibility measurements on Rb_2CsC_{60} (*1*) and extension of the $T_c(P)$ experiments to higher pressure.

REFERENCES AND NOTES

1. R. M. Fleming *et al.*, *Nature* **352**, 787 (1991).
2. G. Sparn *et al.*, *Science* **252**, 1829 (1991).
3. J. E. Schirber *et al.*, *Physica C* **178**, 137 (1991).
4. G. Sparn *et al.*, unpublished results.
5. J. P. McCauley, Jr., *et al.*, *J. Am. Chem. Soc.* **113**, 8537 (1991).
6. O. Zhou *et al.*, *Nature* **351**, 632 (1991).
7. Q. Zhu *et al.*, *Science* **254**, 545 (1991).
8. We first checked that no degradation in x-ray profiles occurred after immersing M_3C_{60} powder in these liquids for several days. Mineral oil was used only below 8 kbar because of its low glass-transition pressure. The disadvantage of pentane-isopentane is its high vapor pressure, which makes it more difficult to seal the cell without trapping voids in the gasket hole.
9. J. Jayaraman, *Rev. Mod. Phys.* **55**, 1 (1983); L. Finger and H. Hazen, *Comparative Chemistry* (Wiley, New York, 1982).
10. J. E. Fischer *et al.*, *Science* **252**, 1288 (1991).
11. H. Zabel, in *Graphite Intercalation Compounds, Topics of Current Physics*, H. Zabel and S. A. Solin, Eds. (Springer-Verlag, Berlin, 1990), pp. 101–156.
12. S. J. Duclos *et al.*, *Nature* **351**, 380 (1991).
13. F. C. Zhang, M. Ogata, T. M. Rice, *Phys. Rev. Lett.* **67**, 3452 (1991).
14. M. Schluter, M. Lannoo, M. Needels, G. Baraff, D. Tomanek, unpublished results.
15. C. M. Varma, J. Zaanen, K. Raghavachari, *Science* **254**, 989 (1991).
16. S. C. Erwin and W. E. Pickett, *ibid.*, p. 842.
17. P. A. Heiney *et al.*, *Phys. Rev. Lett.* **66**, 2911 (1991).
18. G. A. Samara *et al.*, *ibid.* **67**, 3136 (1991).
19. G. Kriza *et al.*, *J. Phys. I (France)* **1**, 1361 (1991).
20. P. W. Stephens *et al.*, *Nature* **351**, 632 (1991).
21. R. Tycko *et al.*, *Science* **253**, 884 (1991).

22. We thank G. Sparn for providing his raw $T_c(P)$ data, M. Y. Jiang for technical assistance, and also K. S. Liang for the use of the X10B beamline. We acknowledge helpful discussion with S. C. Erwin, A. B. Harris, and E. J. Mele. Supported by NSF grants no. DMR-88-19885 and no. DMR-89-01219 and by the Department of Energy, grant no. DE-FC02-86ER45254.

18 November 1991; accepted 2 January 1992

Molecular Dynamics Simulations of Dimer Opening on a Diamond {001}(2×1) Surface

BARBARA J. GARRISON,* ERIC J. DAWNKASKI, DEEPAK SRIVASTAVA, DONALD W. BRENNER*

Computer simulations of hydrocarbon and related molecules using empirical force fields have become important tools for studying a number of biological and related processes at the atomic scale. Traditional force fields, however, cannot be used to simulate dynamic chemical reactivity that involves changes in atomic hybridization. Application of a many-body potential function allows such reactivity to occur in a computer simulation. Simulations of the reaction of small hydrocarbon molecules adsorbed on a reconstructed diamond {001}(2×1) surface suggest that these hydrocarbons are highly reactive species and that initial stages of diamond growth proceed through a dimer-opening mechanism. Rates estimated from transition state theory of two interconversions between states where the dimer is open and closed are given.

CHEMICAL REACTIONS ARE DEFINED by a changing atomic coordination associated with the breaking and making of bonds. Creation of a microscopic description of the events associated with these processes for small systems (*1*) has been a tour de force for modern chemistry. We understand in exquisite detail reaction mechanisms, quantum mechanical resonances, and final vibrational state distribution of reactions such as F + H_2 → FH + H and H + H_2 → H_2 + H. Analogous accomplishments for large ensembles of atoms and molecules have been slow, however, as the focus of research changes from small molecular systems to large ones. Thus, it is timely to question how reactions proceed in condensed phases. To approach this problem, we have used molecular dynamics (MD) calculations to investigate the diamond film formation from hydrocarbon species.

B. J. Garrison, E. J. Dawnkaski, D. Srivastava, 152 Davey Laboratory, Department of Chemistry, Pennsylvania State University, University Park, PA 16802.
D. W. Brenner, Code 6179, Naval Research Laboratory, Washington, DC 20375.

*To whom correspondence should be addressed.

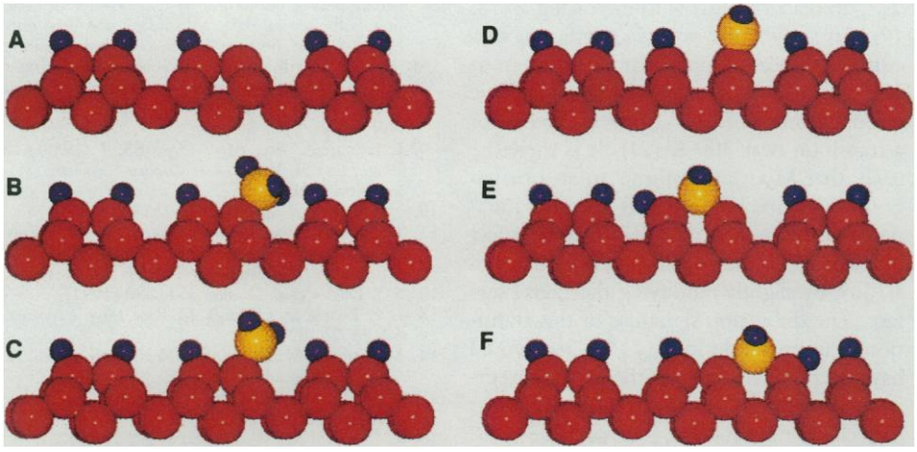

Fig. 1. Side view of the {001}(2×1) surface. In all cases the C atoms are represented by the larger spheres and the H atoms by the smaller spheres. The view angle is slightly off head-on. (**A**) Three surface dimers with an H atom on each dangling bond. (**B**) Surface dimer with a CH_3 replacing an H atom on the dangling bond. (**C**) Surface dimer with a CH_2 replacing an H atom on the dangling bond. (**D**) Same as (C) except that the surface dimer is open. (**E**) Insertion of the CH_2 into the dimer bond. (**F**) Insertion of the CH_2 into the trough position.

A promising approach for examining complex chemical reactions is to integrate Newton's classical equations of motion in time to obtain a movie of the evolving events. Albeit based on ideas formulated 300 years ago, MD simulations continue to be widely used in modern chemistry. The underlying problem in performing realistic MD simulations is to determine or acquire an interaction potential function (actually the solution to the electronic Schrödinger equation within the Born-Oppenheimer approximation) that describes the appropriate chemical forces for all the atoms.

One approach to determining analytic atomic interaction potentials has recently been developed for modeling reactions of hydrocarbon molecules (*2*). The formalism, which was originally derived from chemical pseudopotential theory (*3*), is based on the assumption that potential energy can be written in a form similar to a pair potential (*4*)

$$E = \Sigma_i \Sigma_{j>i} [V_r(r_{ij}) - B_{ij} V_a(r_{ij})]$$

The functions V_r and V_a represent pair-additive repulsive and attractive interactions, respectively; r_{ij} is the scalar distance between atoms i and j; and B_{ij} is a many-body empirical bond order function that may depend on quantities such as atomic coordination and bond angles (*4*). In this approach the pair-additive terms are assumed to be transferable among different bonding environments for a given element, and consequently the many-body effects are built into the bond order function B_{ij} (*3, 4*). One set of pair-additive terms is assumed between each type of atom, and a single analytic expression for the bond order is fit to different atomic hybridizations. Thus, rather than being preassigned as in a traditional force field (*5*), the bonding nature and hybridization of each C atom is determined by the local environment of neighboring atoms and can change during the simulation if the energetics and dynamics dictate that it should do so. This approach removes a major constraint that is inherent in most force field–based hydrocarbon potential functions in that chemical reactivity involving changes in atomic hybridization can be modeled.

The specific functional forms and parameters used in the present simulation were fit to the lattice constant, cohesive energy, and vacancy formation energy of diamond and graphite lattices as well as the length and energy of molecular C–C and C–H bonds (*2*). The function also includes terms that inhibit rotation about dihedral angles for C=C (*6*). As discussed in (*2*), the potential energy function yields reasonable predictions for a wide range of both molecular and surface properties. For example, atomization energies for hydrocarbon molecules ranging from alkanes to large aromatic molecules to radicals are predicted to within 1% or better for over 80% of the molecules examined. The same function also predicts that the (2×1) π-bonded chain reconstruction on the {111} surface is energetically preferred for a clean surface, in agreement with local-density functional calculations (*7*), and correctly predicts that H adsorption is favored on a bulk-terminated surface over adsorption on the π-bonded chain reconstruction (*8*). It also predicts a surface relaxation around a radical on the {111} surface that agrees with recent ab initio cluster calculations (*9*). For the case where the dimer-reconstructed diamond {001} surface is H-terminated, the function yields energetics and dimer bond lengths that agree with predictions from molecular mechanics calculations (*2, 10*). It also yields reasonable predictions for barriers for reactions such as H abstraction (*2*). Taken together, these qualities suggest that this function provides a good description of energetics and bonding for a wide range of diamond surface structures.

We chose to investigate diamond film growth as a model example because it is a complex chemical reaction event that involves many atoms yet is restricted to only two elements, C and H. Understanding the underlying mechanisms of the growth of diamond-like films at low temperatures and pressures is essential for expanding the practical aspects of the technology (*11*). Experimentally a gaseous mixture of hydrocarbon species and H atoms are created above a substrate, commonly diamond itself. Hydrogen atoms are present in abundance and presumably saturate most of the exposed C atoms on the growing diamond surface. In addition, the gas phase H atoms may extract H atoms from the surface to form gaseous H_2 (an exothermic process). The dominant hydrocarbon species (*12*) appear to be acetylene molecules, C_2H_2, and methyl radicals, CH_3. In consideration of these reactants, mechanisms have been proposed for the diamond film growth process on the {111} (*13*), {110} (*14*), and H-terminated unreconstructed {001} (*15*) surfaces. For the {001} surface, however, a recent study indicates that growth may actually occur on a dimer-reconstructed face (*16*). This growth mode is supported by recent MM3 calculations that suggest that the fully hydrogenated surface is thermodynamically unstable with respect to at least partial dimer reconstruction (*10*). Obviously, a dimer-opening mechanism is necessary to initiate the growth on the {001}(2×1) surface.

We examined the reaction pathways after $-CH_x$ adsorption on the {001}(2×1)H surface of diamond. The {001}(2×1) surface is a reconstruction such that C atoms at the surface (2.52 Å separation in the bulk) bond to form surface dimers (1.41 Å separation on the clean surface) as shown in Fig. 1A. This bonding configuration leaves a radical orbital on each surface C atom. The H-terminated surface is formed by the placement of an H atom at each radical site. Because there is a highly strained bond, we believe this surface might exhibit interesting chemistry.

One can determine the dynamics of the system of atoms by integrating the equations of motion for all the particles as a function of time (*17*). The forces for the motion are determined by the many-body hydrocarbon interaction potential. We used

a slab of eight layers of C atoms with 32 atoms per layer, with the {001} face exposed, reconstructed into the (2×1) dimerized surface, and then terminated with H atoms. The top three C layers and all adspecies experienced only the forces due to the interaction potential. In addition to the forces from the interaction potential, the next three layers experienced stochastic forces in order to maintain a desired temperature (*18*). The final two layers were held rigid to keep the bottom from reconstructing. To examine different reaction pathways, we replaced one of the H atoms by either a –C, –CH, $-CH_2$, or $-CH_3$ species. The dynamical response of the ensemble of particles was then computed at simulation temperatures of 1500 to 2500 K (*19*).

The initial adspecies investigated was $-CH_2$. This adspecies could arise either from the direct adsorption of methylene, CH_2 (Fig. 1C), from the gas phase onto a radical site or from an H atom abstraction from a $-CH_3$ adspecies (Fig. 1B). For the empirical potential, the energy cost to remove an H atom from the dimer site is 4.4 eV but is only 4.0 eV from the adsorbed methyl species. The reaction steps suggested by the MD simulation for the $-CH_2$ adspecies case are as indicated in Fig. 1, C to E. In the initial state (Fig. 1C), the atoms surrounding the adsorbate C atom are nearly planar, indicating that it is a radical species. The C–C surface dimer bond is highly strained as these two C atoms were originally next-nearest neighbors in bulk diamond. The next step involves the evolution of an ethylenic configuration (Fig. 1D). The strained C–C dimer bond is broken, and by the arrangement of the atoms a double bond is formed between the adsorbed CH_2 and the surface C atom. The surface radical species is now on the left C atom. Finally, the CH_2 inserts into the middle of the original strained C–C dimer bond (Fig. 1E). The H atoms in the ethylenic adspecies are perfectly aligned for the inserted configuration, and the C atom on the right side of the dimer has a radical orbital. The C atom with the radical site is restricted from having a planar geometry by the presence of neighboring C atoms in the bulk. Another radical site is present for subsequent reactions, perhaps with an H atom that is present in abundance. These reaction steps follow solely from the predictions of the MD simulations.

The insertion reaction was observed for all CH_x adspecies where $x < 3$. The CH_3 species could not insert, as the dimer opening step is highly endothermic. The MD simulations predict that the –CH adspecies is more reactive than the $-CH_2$ adspecies and that atomic C was the most reactive. These predictions are consistent with the energetics of the various states as evaluated by the many-body interaction potential.

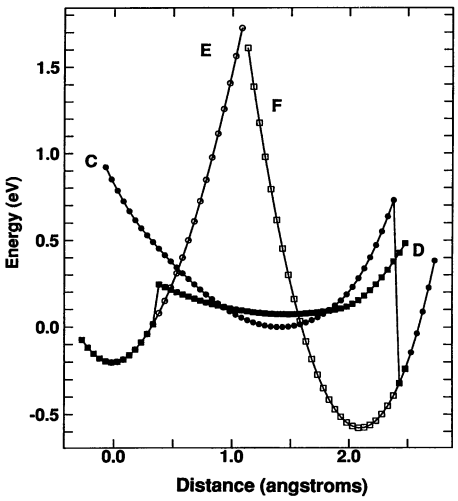

Fig. 2. Constrained potential energy curves for states C, D, E, and F of Fig. 1. The horizontal axis is the distance of the constrained C adspecies from the center of the original dimer, and the vertical axis is the relative energy of the states. For each minimum energy configuration, the values of the horizontal position of the C adspecies, the vertical position, and the relative energy are given: ●, state C (1.43 Å, 1.29 Å, 0.00 eV); ■, state D (1.48 Å, 1.28 Å, 0.07 eV); ○, state E (−0.02 Å, 1.08 Å, −0.20 eV); and □, state F (2.08 Å, 0.92 Å, −0.58 eV).

In order to assess the ease of transitions among the states shown in Fig. 1, we generated potential energy curves for each of the CH_2 adsorption states. The horizontal position of the adsorbed C atom in the surface plane was constrained, and then the remaining atom positions (including the two H atoms on the C adspecies) along with the height of the C adspecies were dynamically relaxed (*20*). In other words, the energy is calculated for positions from left to right in the configurations in Fig. 1 with the C adspecies always in the plane of the surface dimers. The CH_2 adspecies (state C) and ethylenic (state D) configurations have minima positions and energies that are close to each other. The minimum in the potential curve for the inserted configuration (state E) is lower in energy than minima of either the CH_2 adspecies or ethylenic configurations. In the course of the minimization calculations, a fourth state was found (Fig. 1F). This state corresponds to the CH_2 species bonding to a C atom across the trough between the dimer rows, and thus the dimer on the right must be open.

A further analysis of the results of the MD simulations in conjunction with the constrained potential curves shown in Fig. 2 is in order. MD calculations of direct CH_2 adsorption on the {001}(2×1) surface with one radical orbital showed that only the CH_2 adspecies and the ethylenic states, C and D, respectively, were directly accessed. Once the CH_2 adsorbed, the MD calculations exhibited facile transitions to the ethylenic state and occasional transitions (within tens of picoseconds at 1500 to 2500 K) to the inserted state, E. State F was not observed in this time scale by the MD calculations even though it is lowest in energy. To explain this in terms of the energetics, each crossing of the potential curves in Fig. 2 must be analyzed to determine if it is a true crossing of states (facile transition) or a transition state. The two points where states C and D cross are true crossings. There is about a 0.11-eV energy difference for the transition from the CH_2 adspecies state to the ethylenic state. The apparent crossings between C, D and E, F are fictitious because of the constrained dynamics. For example, to get from state C to state F, the dimer on the right must be opened. There are, however, transition states between states D and E and between states C and F.

Simplified transition state theory (*20, 21*) can be used to estimate the rates for these two transitions. Using equation 1 of (*20*), one gets $k_{D\rightarrow E} = 6.9 \times 10^{11} \times \exp(-0.17\ \text{eV}/kT)\ \text{s}^{-1}$ and $k_{C\rightarrow F} = 3.0 \times 10^{12} \times \exp(-0.73\ \text{eV}/kT)\ \text{s}^{-1}$, where k is the Boltzmann constant and T is temperature. The D → E transition is extremely easy and has a lifetime of approximately 1 ns at room temperature. The transition C → F is much slower and has a minimum lifetime of 0.5 s at room temperature. The transition C → F is not observed in these MD simulations because the concentration of species in state C is preferentially drained into state D and then into state E. Within the approximations of this empirical potential, the predicted barriers are upper bounds in that some of the atomic positions are constrained.

The series of states and reaction mechanisms shown in Fig. 1 present an interesting concept to the dimer-opening step in diamond film growth on the {001} surface. First, the $-CH_2$ radical is an important adspecies. The origin of the $-CH_2$ can either be from direct adsorption or H abstraction from a CH_3 adspecies. Second, because the surface is assumed to be dimer-reconstructed, the steric hindrance problems (*10*) associated with the Harris (*15*) mechanism for CH_3 are significantly reduced. Finally, and perhaps most important, there are variants of these motions that are close in energy. For example, state F might be readily formed if the dimer on the right were replaced by a single C atom or a step edge. Therefore, a perfect {001}(2×1) surface is not needed for this basic concept of atomic motions to operate.

Molecular dynamics simulations for reactions of hydrocarbons using an empirical potential are now possible. Changes in

bonding environment occur dynamically during the simulations. This approach opens the door for proposing reaction pathways that involve rehybridization of C atoms in molecules. For diamond film formation we have suggested that $-CH_2$ species are highly reactive and may be important for growth. The resulting pictures present a challenge to experimentalists for laboratory confirmation and to theorists for calculating the energetics by first-principle methods (*22*).

REFERENCES AND NOTES

1. *Chem. Eng. News* **68** (no. 23), 32 (4 June 1990).
2. D. W. Brenner, *Phys. Rev. B* **42**, 9458 (1990).
3. G. C. Abell, *ibid.* **31**, 6184 (1983).
4. J. Tersoff, *Phys. Rev. Lett.* **56**, 632 (1986); *Phys. Rev. B* **37**, 6991 (1988).
5. U. Burkert and N. L. Allinger, *Molecular Mechanics* (American Chemical Society, Washington, DC, 1982); S. Weiner, P. Kollman, D. Nguyen, D. Case, *J. Comput. Chem.* **7**, 230 (1986); B. Brooks *et al.*, *ibid.* **4**, 187 (1983); K. D. Gibson and H. A. Scheraga, *ibid.* **8**, 826 (1987); N. L. Allinger, F. Li, L. Yan, J. C. Tai, *ibid.* **11**, 868 (1990); W. L. Jorgensen and J. Tirado-Rives, *J. Am. Chem. Soc.* **110**, 1657 (1988); C. F. Wong and J. A. McCammon, *ibid.* **108**, 3830 (1986).
6. D. W. Brenner, J. A. Harrison, C. T. White, R. J. Colton, *Thin Solid Films*, in press.
7. D. Vanderbilt and S. G. Louie, *Phys. Rev. B* **30**, 6118 (1981).
8. A. V. Hamza, G. D. Kubiak, R. H. Stulen, *Surf. Sci.* **206**, L833 (1988).
9. M. Page and D. W. Brenner, *J. Am. Chem. Soc.* **113**, 3270 (1991).
10. Y. L. Yang and M. P. D'Evelyn, *ibid.*, in press.
11. *J. Mater. Res.* **5** (November 1990).
12. F. G. Celii, P. E. Pehrsson, H.-T. Wang, J. E. Butler, *Appl. Phys. Lett.* **52**, 204 (1988).
13. M. Frenklach and K. E. Spear, *J. Mater. Res.* **3**, 133 (1988); D. Huang, M. Frenklach, M. Maroncelli, *J. Phys. Chem.* **92**, 6379 (1988); M. Tsuda, M. Nakajima, S. Oikawa, *J. Am. Chem. Soc.* **108**, 5780 (1986).
14. W. A. Yarbrough, Diamond Optics IV, *SPIE Proc. 1534*, in press; D. N. Belton and S. J. Harris, *J. Chem. Phys.*, in press.
15. S. J. Harris, *Appl. Phys. Lett. B* **56**, 2298 (1990).
16. T. Tsuno, T. Imhi, Y. Nishibayashi, K. Hamada, N. Fujimore, *Jpn. J. Appl. Phys.* **30**, 1063 (1991).
17. D. W. Brenner and B. J. Garrison, *Surf. Sci.* **198**, 151 (1988); D. Srivastava, B. J. Garrison, D. W. Brenner, *Phys. Rev. Lett.* **63**, 302 (1989); *Langmuir* **7**, 683 (1991).
18. S. A. Adelman and J. D. Doll, *J. Chem. Phys.* **64**, 2375 (1976); R. R. Lucchese and J. C. Tully, *Surf. Sci.* **137**, 570 (1983); H. J. C. Berendsen, J. P. M. Postma, W. F. van Gunsteren, A. Dinola, J. R. Haak, *J. Chem. Phys.* **81**, 3684 (1984).
19. Absolute temperature calibration is difficult with empirical potentials because most are not fit to the melting temperature. In addition, because of the exponential dependence of most reaction rates on temperature, it is quicker to examine reaction mechanisms at higher temperatures.
20. D. Srivastava and B. J. Garrison, *J. Chem. Phys.* **95**, 6885 (1991).
21. A. F. Voter, *Phys. Rev. B* **34**, 6819 (1986).
22. After submission of this manuscript, a preprint (D. Huang and M. Frenklach, *J. Phys. Chem.*, in press) was called to our attention. Using semiempirical electronic structure calculations, they examined a reaction pathway similar to C to E, although with a different transition state.

23. Supported by the Office of Naval Research, the National Science Foundation, and a Teacher-Scholar Award to B.J.G. from the Camille and Henry Dreyfus Foundation. Pennsylvania State University supplied a generous grant of computer time for these studies. D.W.B. is supported by the Office of Naval Research through the Naval Research Laboratory.

21 October 1991; accepted 3 December 1991

Structure of Transcription Elongation Complexes in Vivo

MARK KAINZ AND JEFFREY ROBERTS

The opening of duplex DNA in the elongation phase of transcription by *Escherichia coli* RNA polymerase in vivo was detected at a regulatory site where a prolonged pause in transcription occurs. Single-stranded DNA in the transcription bubble was identified by its reactivity with potassium permanganate ($KMnO_4$). The elongation structure in vivo was similar to that of transcription complexes made in vitro with some differences. The observed reactivity to $KMnO_4$ of the DNA template strand was consistent with the existence of an RNA-DNA hybrid of about 12 nucleotides.

THE COMPLEX OF RNA POLYMERASE (RNAP), DNA, and the elongating mRNA transcript is an intermediate in the enzymatic reaction and the site of the regulatory processes of termination and antitermination. The elongation complex of *Escherichia coli* RNAP has the following properties in vitro: (i) its footprint is more compact than that of initiation complexes (20 to 30 bp versus 65 to 95 bp) (*1, 2*); (ii) base-specific contacts are not evident (*1*); (iii) the DNA (~17 bp) is unwound in the transcription bubble (*3*); and (iv) the DNA template and the nascent RNA form a hybrid of 10 to 12 bp (*4–6*), although this value has been questioned (*7*).

During transcription in vitro of the *E. coli* bacteriophage λ late gene operon (*8*) and the late gene operons of related phages 82 (*9*) and 21 (*10*), RNA polymerase pauses after making only 15 to 25 nucleotides of RNA, at a position specific to each phage DNA. These paused elongation complexes are the substrates on which each phage gene Q-encoded antiterminator protein acts in vitro to modify RNAP. We have identified the paused elongation complexes in vivo, and have used them to study the structure of the elongation complex in vivo.

We detected paused complexes in cells using $KMnO_4$ to modify thymines and cytosines in denatured DNA (*11*) and thus to mark the transcription bubble. Cells bearing plasmids with the late promoter and initially transcribed region of the late operon of λ or related phages were treated with $KMnO_4$ during growth, and $KMnO_4$-modified pyrimidines were detected by primer extension. In some experiments the drug rifampicin, which prevents initiation but not elongation of transcription by *E. coli* RNA polymerase, was added before $KMnO_4$ treatment. Inhibition of initiation allows elongating and paused RNAP to clear the DNA and thus identifies such enzymes, and also freezes RNAP at the promoter in the open complex.

We analyzed three plasmids containing the λ late operon: (i) pXY306 (*12*) contains the wild-type λ promoter p_R' with its associated regulatory sequence *qut* (for "Q utilization"); (ii) pXY306 (+6C) is a *qut*$^-$ point mutant that does not support the in vitro pause at $^+16$–$^+17$ (and cannot be modified by Q), but still has an active promoter (*13–15*); and (iii) pXY306 (−11G) contains a mutation that nearly abolishes promoter function (*13*). Wild-type pXY306 has reactive residues at positions +1 and +2 of the bottom (template) strand, and +14, +15, and +16 of the top (nontemplate) strand (Fig. 1A) (*16*). Treatment with rifampicin alters this pattern in two ways. Reactivity at +1 and +2 (lane 2) and +14, +15, and +16 (lane 8) is abolished, and the minor reactivity of T at −11 (lane 2) and −2, −6, −7, and −8 (lane 8) increases. We infer that bases at +1 and +2 on the bottom strand and at +14, +15, and +16 on the top strand occur in single-stranded regions of the transcription bubble of RNA polymerase paused after making 16 or 17 nucleotides of the late RNA, whereas T at −11 on the bottom strand and −2, −6, −7, and −8 on the top strand are present in single-strand regions of open complex formed at the promoter. Open and paused complexes coexist in a population, although for steric reasons they probably could not exist on the same DNA molecule. A time course shows that the half-life of the paused complex in vivo is about 30 s (*17*).

This identification of melted DNA in open and paused complexes was supported by analysis of the mutant plasmids. $KMnO_4$ treatment of cells bearing pXY306 (+6C) detected reactivity ascribed to open complex [at −11 (Fig. 1A, lane 3) and weakly at −2,

Section of Biochemistry, Molecular, and Cell Biology, Biotechnology Building, Cornell University, Ithaca, NY 14853.